Journal of Materials Chemistry A

ROYAL SOCIETY OF CHEMISTRY

PAPER

View Article Online
View Journal | View Issue

Cite this: J. Mater. Chem. A, 2025, 13, 16204

Identifying rate-limiting steps in photocatalysis: a temperature-and light intensity-dependent diagnostic of charge supply *vs.* charge transfer†

Yohei Cho, * Kyo Yanagiyama, Poulami Mukherjee, Panitha Phulkerd, Krishnamoorthy Sathiyan, Emi Sawade, Toru Wada and Toshiaki Taniike *

Photocatalysis fundamentally relies on two interconnected processes: charge supply, which includes carrier generation, separation, and migration, and charge transfer, which involves interfacial redox reactions driving chemical transformations. Differentiating these two processes is critical, as addressing the wrong bottleneck can lead to ineffective optimization strategies. Here, we introduce a simple yet powerful diagnostic based on the distinct temperature sensitivities of these two processes. While charge transfer follows Arrhenius-type kinetics and accelerates significantly with increasing temperature, charge supply is comparatively temperature-insensitive. By systematically varying both temperature and light intensity, we pinpoint the Onset Intensity for Temperature Dependence (OITD), the threshold where surface reactions begin to bottleneck overall photocatalysis. Applying this method to ZnO and TiO_2, it is revealed that ZnO has sufficient carrier generation but sluggish surface reactions, whereas TiO_2 suffers from insufficient carrier supply at lower irradiance. Experiments with TiO_2 powders of varying crystallinity and morphology reveal that smaller particles, which ensure better surface accessibility within the carrier's mean free path, contribute more to performance improvements than enhanced crystallinity. By clarifying which step actually limits performance, this approach provides a straightforward roadmap for targeted catalyst optimization and a deeper understanding of key processes in photocatalysis.

Received 16th January 2025
Accepted 10th April 2025

DOI: 10.1039/d5ta00415b

rsc.li/materials-a

1. Introduction

Photocatalysis is a promising solution to address energy and environmental challenges, enabling processes such as solar-driven water splitting, carbon dioxide reduction, and pollutant degradation.[1–3] The widely accepted mechanism involves four main steps: (i) photon absorption at semiconductor to generate electron–hole pairs, (ii) charge separation, (iii) charge carrier migration to the semiconductor surface, and (iv) charge transfer where these carriers drive redox reactions.

Many studies focus on two major strategies, band engineering[4–8] and surface modification,[1,9,10] to enhance overall performance. However, without identifying the specific step that critically limits efficiency, these strategies may be applied somewhat randomly, leading to inefficient material development. For instance, if there is not enough charge at the photocatalyst surface, improving the charge transfer kinetics will have only a limited impact. Conversely, if the surface charge is already sufficient, narrowing the bandgap should not be the top priority; instead, charge transfer kinetics must be improved first. Therefore, it is imperative to identify the true performance bottleneck before selecting and implementing the most appropriate strategy.

Considering that photocatalysis is addition of charge transfer step to dark catalysis, the primary concern becomes whether there are sufficient charge carriers available at the surface. To thoroughly discuss this, it is rational to divide the photocatalytic process into two main categories: (1) charge supply, which includes carrier generation, separation, and migration, and (2) surface charge transfer, referring to the interfacial redox reactions (Fig. 1a). If charge carriers are in excess (charge transfer-limited), the excited carriers reaching the surface cannot react before recombining, resulting in reduced overall photocatalytic performance. In such cases, the design strategy should focus on improving the charge transfer kinetics. Conversely, if there is a shortage of excited carriers, enhancing light absorption, carrier separation, or migration becomes more critical, as enhancing charge transfer kinetics is meaningless without excited carriers to transfer.

Herein, we propose a diagnostic method to discern whether a given photocatalyst is primarily limited by charge supply or by charge transfer. As demonstrated in Fig. 1b, in our approach, the light intensity is systematically increased from low to high

Graduate School of Advanced Science and Technology, Japan Advanced Institute of Science and Technology, 1-1 Asahidai, Nomi, Ishikawa 923-1292, Japan. E-mail: yohei-c@jaist.ac.jpToshiaki; taniike@jaist.ac.jp

† Electronic supplementary information (ESI) available. See DOI: https://doi.org/10.1039/d5ta00415b

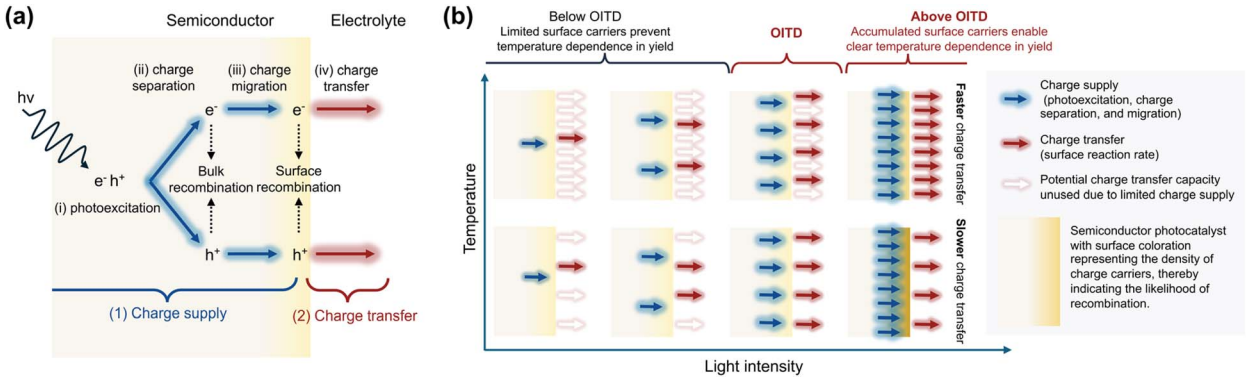

Fig. 1 (a) Comparison of definitions of "charge supply" and "charge transfer" with the commonly accepted photocatalysis mechanism. The charge supply includes three steps, photoexcitation, charge separation, and charge migration. (b) Simplified schematic illustration of the diagnostic approach used to determine whether a photocatalyst is limited by charge supply (blue arrows) or charge transfer (red arrows). As light intensity increases from left (low) to right (high), the system transitions from insufficient to surplus carriers, as shown in the increase of blue arrows. Temperature is varied in parallel, selectively accelerating the charge transfer process, which is represented by the increase in red arrows from four at low temperature to eight at high temperature. Below the Onset Intensity for Temperature Dependence (OITD), the red arrows remain the same at different temperatures due to the limited charge supply. Unfilled arrows indicate unused potential for charge transfer due to insufficient charge supply. Once the light intensity exceeds the OITD, additional carriers enable a noticeable increase in the red arrows, demonstrating stronger temperature dependence in the photocatalytic reaction. By examining the behavior below and above the OITD, one can discern whether the performance is governed primarily by charge supply or by charge transfer.

so that the photocatalyst transitions from a state of insufficient carriers to a state of overabundance. The key point of this approach is controlling the temperature, which selectively accelerates charge transfer because it follows an exponential dependency on temperature, as described by the Arrhenius equation.[11] In contrast, the supply of photoexcited carriers is relatively insensitive to temperature, owing to the inherent temperature insensitivity of semiconductor excitation processes and the fixed population of generated carriers.[12] As a result, once the generated carriers become plentiful, the faster charge transfer at higher temperature reveals its effect on the overall photocatalytic performance. We define the light intensity at which the temperature dependence begins to emerge as the Onset Intensity for Temperature Dependence (OITD). By analyzing the OITD and the behavior beyond this point, we can determine whether a photocatalyst's performance is governed by charge supply or charge transfer.

We demonstrate this diagnostic method by performing photocatalytic degradation of methylene blue (MB) under systematically varied light intensities (from 2 to 250 W m^{-2}) and controlled temperatures (10 and 40 °C). First, we compare TiO_2 and ZnO as representative photocatalysts, then extend our analysis to a series of TiO_2 samples calcined at various temperatures to illustrate how this approach can guide rational catalyst design.

2. Experimental

2.1 Material preparation

TiO_2 and ZnO samples were prepared by first dissolving a specified amount of the precursor in absolute ethanol for titanium tetrabutoxide ($Ti(OCH_2CH_2CH_2CH_3)_4$) and in deionized water for zinc nitrate ($Zn(NO_3)_2$). Citric acid (CA) was then added to achieve a metal-to-CA molar ratio of 0.5 : 1.0. Each solution was stirred for 30 minutes at 60 °C to ensure homogeneity, with the TiO_2 preparation performed under an inert atmosphere to prevent unwanted reactions. Before calcination, the solutions were kept for evaporation at 100 °C for 3–4 hours. Calcination of the TiO_2 precursor was carried out at 600 °C for 4 hours, while the ZnO precursor was calcined at 1000 °C for 4 hours. Separately, a series of TiO_2 samples were synthesized by dissolving titanium tetrabutoxide in absolute ethanol, followed by calcination at different temperatures ranging from 450 °C to 850 °C in 50 °C intervals, each for a duration of 1 hour.

2.2 Photocatalytic performance evaluation

The photocatalytic performance of the synthesized samples was evaluated in an aqueous solution using MB as a model reactant.[13] The concentration of MB in the solution was set to 6.7 ppm. For each measurement, 100 μg of photocatalyst powder was dispersed in a total solution volume of 300 μL. The reaction was carried out using a Peltier-based temperature controller placed at the bottom of the reactor. The set temperatures of 10 °C and 40 °C corresponded to measured temperatures of 12.9 ± 0.3 °C and 39.2 ± 0.5 °C, respectively, but are referred to as 10 °C and 40 °C for simplicity in this paper (Fig. S1†). Six measurements ($N = 6$) were performed for each set of conditions and samples to ensure reproducibility. A Xe lamp (Suntest CPS+, Atlas) was used as a light source, and the light intensity was varied between 2 and 250 W m^{-2} using neutral density (ND) filters. The specifications for the ND filters are provided in Fig. S2–S4.† The MB decomposition during irradiation was measured using a plate reader (Epoch 2, Bio-Tek), where the decrease in the absorbance of MB at its peak absorption wavelength of 665 nm was tracked, with the background set to the absorbance at 800 nm. The MB decomposition over time was fit to first-order kinetics, expressed as:

$$C_t = C_0 \exp(-kt), \quad (1)$$

where $C_t$is the concentration of MB at time t, $C_0$is the initial concentration, and k is the rate constant.

To account for MB photolysis in the absence of photocatalyst, the corresponding decay rate (k_{MB}) was measured *via* control experiments. The net photocatalytic rate (k_{net}) was then determined by subtracting k_{MB} from the overall observed rate (k_{obs}):

$$k_{net} = k_{obs} - k_{MB}, \quad (2)$$

For reference, the decay rate of MB alone (k_{MB}) is plotted in Fig. S5 in the ESI,† where further details on the control experiments and temperature effects are also provided.

3. Results

3.1 Comparison between TiO_2 and ZnO

To illustrate the concept, we first conducted experiments using TiO_2 and ZnO, both well-established photocatalysts. Reactions were performed under controlled temperatures of 10 and 40 °C while varying the light intensity.

The degradation profiles of MB under an irradiation intensity of 250 W m^{-2} and reaction temperature at 40 °C are shown in Fig. 2a. The profiles are similar between TiO_2 and ZnO, suggesting comparable photocatalytic activities under this condition.

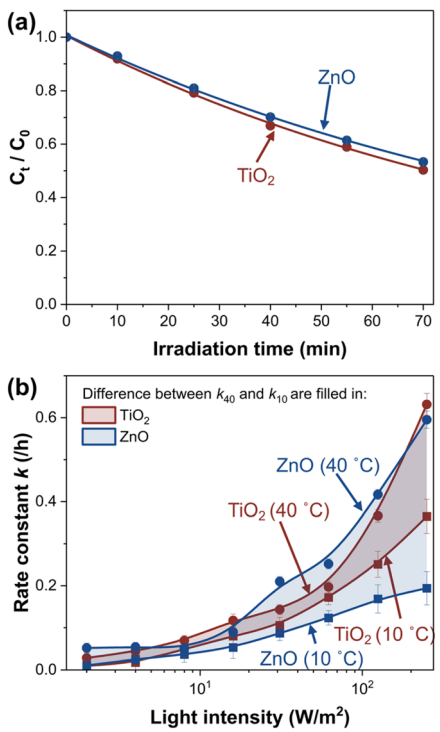

Fig. 2 (a) Degradation profiles of MB under an irradiation intensity of 250 W m^{-2} at 40 °C for TiO_2 and ZnO. Similar degradation profiles mask underlying differences in the rate-limiting steps. (b) Kinetic constants (k) as a function of light intensity and temperature. ZnO shows significant temperature dependence at low light intensities, while TiO_2 exhibits temperature dependence only at higher intensities.

In Fig. 2b, however, it can be observed that two materials behave differently under controlled light intensity and temperature. In the case of ZnO, its photocatalytic performance at 10 °C is relatively low compared to TiO_2. The difference in the kinetics between the two temperatures, OITD, appears at around 20 W m^{-2}. According to the concept illustrated in Fig. 1b, the OITD suggests that the charge supply surpasses surface catalysis, and this threshold intensity is the point at which excess excited carriers at the surface are reacted by faster kinetics at increased temperature. Thus, the low OITD shows charge supply is superior to charge transfers in this photocatalyst, and the low k_{10} performance after the onset shows inefficient surface catalysis.

In contrast, TiO_2 demonstrates a higher kinetic constant than ZnO at 10 °C, and this difference becomes pronounced above 100 W m^{-2}. The OITD for TiO_2 is observed at a higher threshold, around 60 W m^{-2}. Referring to the concept in Fig. 1b, the superior performance in TiO_2 at 10 °C suggests higher charge transfer kinetics relative to ZnO, consuming excited carriers rapidly and minimizing their accumulation on the surface.

Overall, each of the two materials presents distinct bottlenecks. ZnO, with its low performance above OITD, surface catalysis enhancement such as cocatalyst loading would be an effective strategy. The lower OITD is either explained by the low catalysis capability, or by the direct bandgap structure that contributes to higher charge supply.[14] Conversely, TiO_2, possessed higher charge transfer performance as seen in k_{10} above OITD. Building on this observation, strategies to enhance charge supply, including bandgap narrowing or improvements in charge migration, would be promising directions for further optimization. As such, we successfully demonstrate a diagnostic approach to identify whether photocatalytic performance is limited by charge supply or charge transfer, which aligns with the core concept of this work to guide rational catalyst design.

It should be noted that the purpose of this comparison is to demonstrate that even photocatalysts with similar at a certain condition can exhibit distinct behaviors when analyzed through temperature and light intensity dependence and that the TiO_2 and ZnO samples were not synthesized under identical conditions. Thus, for reference, characterization data including surface area and crystallinity are provided in ESI Table S1 and Fig. S6 and S7.† In addition, to ensure that the photocatalyst itself did not degrade during the course of a single measurement—which would undermine the validity of the kinetic analysis—we performed two-cycle tests under the most severe reaction conditions (40 °C, 250 W m^{-2}). As shown in Fig. S8,† the photocatalytic performance remained consistent between the two cycles, confirming the stability of the samples during measurement.

3.2 Comparison between TiO_2 with varying calcination temperatures

To demonstrate the robustness of our diagnostic method and its applicability to more realistic scenarios, we prepared a series

of TiO_2 samples calcined at different temperatures ranging from 450 to 850 °C. Changing the calcination temperature alters several key factors, including surface area, crystallinity, and defects, which remains difficult to understand completely. By controlling reaction temperature and light intensity, we analyzed through the contributions of charge transfer and charge supply, identifying which factors are more critical under specific conditions.

The changes in properties associated with the calcination temperatures were first evaluated. Powder X-ray diffraction (XRD) confirmed that the pure anatase phase retained until 750 °C, and the rutile phase started to appear at higher temperatures (Fig. S9†). Fig. 3a shows particle diameters measured by transmission electron microscopy (TEM) for each calcination temperature, revealing an increase in particle size as the temperature rises. Histograms in Fig. S10† are based on data from approximately 100 particles. The bandgap energies estimated from UV-Vis diffuse reflectance spectroscopy (DRS) remained relatively constant within the anatase phase but decreased with the phase transition to rutile, as shown in Fig. 3b. This decrease is consistent with the narrower bandgap of rutile TiO_2 compared to anatase (the full UV-Vis DRS data are available in Fig. S11†). The Brunauer–Emmett–Teller (BET) surface area analysis (Fig. 3c) shows that samples calcined below 600 °C retain high surface areas due to limited grain growth, while above 600 °C, particle sintering reduces the surface area sharply to around 2–4 $m^2\ g^{-1}$. This reduction in surface area was accompanied by a loss of nanoscale features, observed in the pore size distribution obtained using the Barrett–Joyner–Halenda (BJH) method (inset of Fig. 3c). The N_2 adsorption isotherms are presented in Fig. S12.†

Photocatalytic activities under different calcination temperatures for these TiO_2 under 250 W m^{-2} are presented in Fig. 4a. The temperature dependence, $k_{40} - k_{10}$, is further demonstrated in Fig. 4b. This light intensity exceeds the OITD, as indicated by the temperature and light intensity dependence shown in Fig. S13–S15,† where no clear dependence of the OITD on the calcination temperature was observed under the present experimental conditions and resolution.

Fig. 4 presents following key observations. First, the trend of the kinetic constant changes at a calcination temperature of 600 °C, which aligns with the temperature exhibiting the diminished BET surface area and pore volume. Second, when the calcination temperature is below 600 °C, the kinetic constant increases as the calcination temperature decreases, with a notable rise in reaction temperature dependence, represented by the difference ($k_{40} - k_{10}$). Third, for the samples calcined above 600 °C, the reaction rate constant at both 10 and 40 °C increase slightly with temperature dependence became less, which is reverse of less than 600 °C. Additionally, the phase transformation between anatase and rutile does not appear to significantly impact performance.

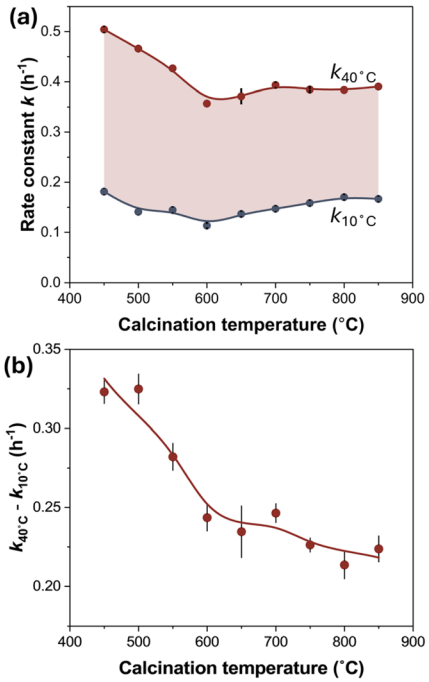

Fig. 4 (a) Photocatalytic reaction rate constants for TiO_2 samples calcined at various temperatures, measured under an irradiance of 250 W m^{-2} at 10 and 40 °C. The gap between the two temperatures has been filled to better illustrate the temperature effect. (b) The difference in reaction rate constants between 40 °C and 10 °C as shown in (a), highlighting the influence of temperature on the reaction.

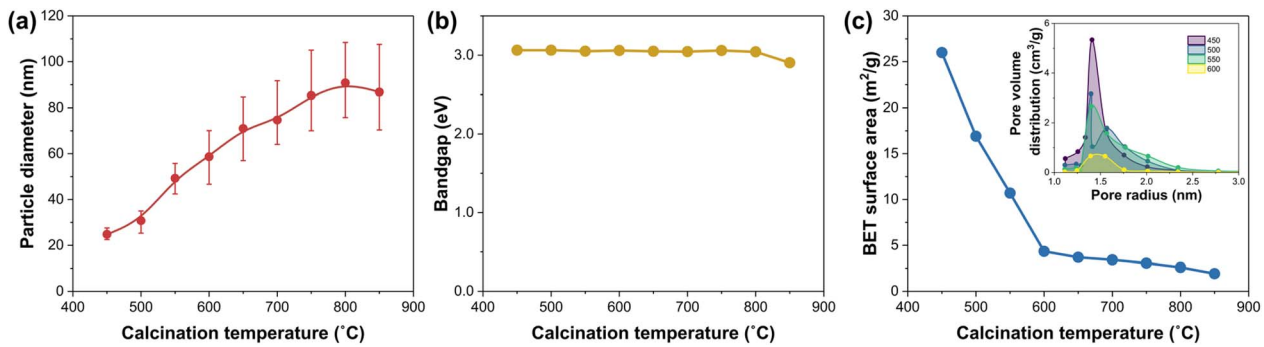

Fig. 3 (a) Particle size for TiO_2 calcined at various temperatures as determined from TEM measurements. (b) Bandgap energies estimated from UV-Vis DRS, showing a decrease with the anatase-to-rutile transition at 850 °C. (c) BET surface areas decrease across the entire temperature range due to particle sintering, sharply up to 600 °C and saturate beyond this point. This is accompanied by a decline in the pore volume (inset).

We first discuss the increase in activity together with significant increase in temperature dependence of reaction rate with decreased calcination temperature below 600 °C. Based on Fig. 1b, above OITD, the excess carriers exist, and the increased charge transfer kinetics with rising temperature consumes these excess carriers, which originates the temperature dependence. Therefore, the high performance below 600 °C together with the high temperature dependence can well be explained by the increased charge supply.

To further understand this phenomenon, we correlate these findings with BET surface area and nanostructure analysis in Fig. 3c. Fig. 5 provides schematic models comparing nanoparticles (Fig. 5a) and a large particle (Fig. 5b). In each model, light is depicted as coming from above, with "+" and "−" symbols representing charges that have reached the surface and yellow dotted circles indicating newly excited carriers and their mean free paths. In the nanoparticle model, more surfaces are included within the mean free path of the excited carriers than the large particle model, resulting in successful charge migration to the surface. This model aligns with the better charge supply and stronger temperature dependency. This distinction indicates that rather than focusing on improving mobility or lifetime *via* enhanced crystallinity, a common discussion, enhancing surface accessibility through nanoparticle formation may be more effective for improving charge supply.[15–17]

We now turn to the calcination temperature above 600 °C. In this region, both k_{10} and k_{40} slightly increase with the rise in calcination temperature; however, the effect of reaction temperature becomes less pronounced, as shown in Fig. 4b. This is the opposite trend observed below 600 °C. The observed increase in k_{10} and k_{40} alongside the reduced temperature dependence suggests that while charge transfer improves, the charge supply does not, resulting in reduced surface-excited carriers. Consequently, when the reaction temperature increases, fewer excited carriers are involved in the reaction, leading to a reduction in overall temperature dependence. Additionally, the lack of a significant increase in charge supply can be understood by referring to Fig. 5b. As the particle size becomes sufficiently large relative to the mean free path of the excited carriers, the particle size effect diminishes. This also implies that the commonly discussed improvement in crystallinity does not significantly contribute to enhancing charge supply.

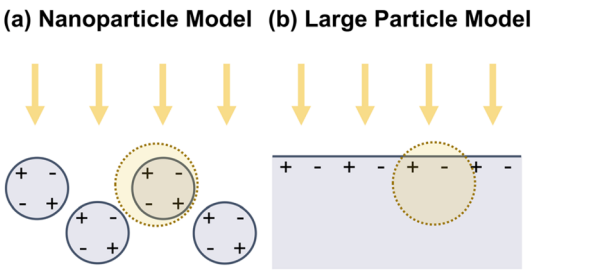

Fig. 5 (a) Schematic of a nanoparticle TiO_2 sample during photocatalytic reactions. (b) Schematic of a large-particle TiO_2 sample during photocatalytic reactions. In both models, light enters from above, with "+" and "−" indicating charges reaching the surface, and yellow dotted circles representing newly excited carriers and their mean free paths.

To discuss the improved charge transfer above 600 °C, it can possibly be explained by the dependence on exposed facets or increased defects. Calcination promotes crystal growth, which may expose facets favorable for charge transfer.[18–21] While further analysis lies beyond the scope of this paper, insights could be gained through analyses of exposed facets or defects.

It should be noted that the kinetic constant is often correlated with large surface areas and a high number of active sites. However, unlike conventional thermal catalysts, increasing the reaction surface area does not simply lead to improved performance. Furthermore, when combined with the discussion on the temperature dependence of reactions, as seen in Fig. 4, improvements in charge supply and charge transfer need to be carefully considered.

As shown in Fig. S8,† in the data used for Fig. 4, only the sample calcined at 450 °C exhibited a slight decrease in performance. According to the XRD results in Fig. S16,† the crystallinity and crystal structure remain largely unchanged before and after the two-cycle reactions. However, the N_2 adsorption isotherms in Fig. S17† and the corresponding BET analysis in Fig. S18† indicate a decrease in BET surface area from 31 to 27 $m^2\,g^{-1}$, along with a slight reduction in hysteresis. These results suggest that partial collapse of mesopores and/or changes in secondary aggregation may have occurred. Nonetheless, these findings do not significantly affect the overall temperature-dependent trends or the main conclusions regarding charge supply and charge transfer.

To summarize, below 600 °C, the effect of charge supply enhancement through nanoparticle formation is significant, with a clear manifestation of temperature dependence. On the other hand, the impact of increased calcination temperature is primarily reflected in improved charge transfer. The commonly discussed improvement in crystallinity appears to have minimal influence on enhancing charge supply.

4. Discussion

The concept introduced in this study enables the differentiation between limitations arising from charge supply and charge transfer kinetics in photocatalytic reactions, which was previously difficult to achieve. Common design strategies like element substitution, doping, and crystal structure control have been used to modify the electronic structure of semiconductors. Besides, photocatalysts are sensitive to various defects.[22] However, these modifications often unintentionally affect surface catalytic properties as well. This overlap makes it challenging to determine whether improvements in photocatalytic performance are due to changes in bulk charge supply properties or alterations in surface charge transfer kinetics. By systematically varying temperature and light intensity, our method would provide an effective means to separate these two factors, offering more precise insights into the factors that enhance performance. Moreover, as demonstrated in the calcination temperature studies of TiO_2, it is often difficult to clarify the origin of photocatalytic activity when changing

synthetic parameters. The proposed method facilitates the identification of whether changes in these parameters predominantly influence charge supply or charge transfer.

The concept of OITD is supported by the recent work using photoelectrochemical measurement together with *in situ* spectroscopic photogenerated holes under steady-state illumination.[11] The study revealed that when temperature increases from 20 to 50 °C under high light intensity (~1 sun), the photocurrent goes up while the monitored surface-hole concentration decreases. This can be explained by the accelerated charge transfer than charge supply, resulting in decreased surface carriers. Consequently, as the light intensity is continuously decreased, the surface charge available for consumption upon increasing the reaction temperature eventually becomes depleted, causing the overall yield to lose its temperature dependence. This marks the threshold at which temperature dependence disappears, which matches the definition of OITD in this work. In addition, these discussions illustrate that mismatches in the rates of charge supply and charge transfer, rather than the specific substrate (MB, water, or any other reactant), govern the onset of temperature-dependent behavior and confirm the broader significance of the OITD concept introduced here.

Several existing studies have investigated charge supply and charge transfer kinetics, yet key differences distinguish our approach. Some of these studies employ transient absorption spectroscopy (TAS) with pulse lasers, which typically use light intensities much higher than those under steady-state illumination. TAS is a powerful tool that tracks the ultrafast dynamics of photogenerated carriers—such as excitation, trapping, recombination, and interfacial charge transfer—by examining the temporal evolution of transient absorption signals.[23,24] While these measurements yield detailed insights into the intrinsic carrier behavior and reaction pathways, they are often conducted under high-intensity excitation conditions that may not directly reflect steady-state photocatalytic performance. In contrast, our method applies continuous illumination at intensities comparable to actual operating conditions, allowing us to directly assess charge supply and charge transfer during the target reaction. This approach provides a more direct means of identifying the rate-limiting process in a given material under realistic conditions.

Additionally, another conventional approach estimates charge supply efficiency by assuming charge transfer efficiency to be 100% in the presence of a sacrificial agent. However, whether charge transfer efficiency truly reaches 100% under such conditions remains uncertain, as not all photogenerated carriers necessarily contribute to the reaction without recombination. Our method, which detects excess carriers through temperature-dependent analysis, offers a more direct and reliable means of evaluating charge supply. This comparison highlights the advantage of our approach in providing mechanistic insights under realistic operating conditions.

To apply this method in catalyst development, we can use the data obtained to guide specific improvements. For catalysts that already show high performance, analyzing their charge supply and charge transfer kinetics can help identify the optimal balance between these factors. We can then focus on replicating these properties in new materials. To enhance charge supply, strategies may include enhancing light absorption, improving charge separation efficiency, increasing charge mobility, and reducing charge trapping.[25] Nano-structuring the photocatalyst, making a nano-particle, nano-rod or nano-wire with a radius comparable to or less than the mean free path can be an effective approach, as supported by the results above.[26] For boosting the charge transfer, methods such as shifting the conduction band more negative and the valence band more positive can be considered, as these increase thermodynamic driving force. Additionally, adding well-known co-catalysts to the photocatalyst surface is a promising strategy to enhance the surface charge transfer kinetics.[9,27,28]

To bridge the general understanding of photocatalysis with our current framework, we need to connect charge supply and charge transfer to the recombination processes, critical in photocatalysis. As illustrated in Fig. 1a, recombination typically occurs in two forms: bulk and surface.[29] Bulk recombination represents the portion of absorbed light that fails to contribute to the charge supply, whereas surface recombination involves charges that reach the surface but fail to transfer to the reactant. Notably, an excess of charges at the surface can intensify surface recombination if the charge supply surpasses the capacity for charge transfer. This perspective also clarifies the behavior around OITD. At intensities lower than OITD, excess carriers are minimal, and surface recombination is not significant. Once the intensity exceeds OITD, surface recombination starts to become noticeable at lower temperatures. With further increases in temperature, a larger fraction of these charges can participate in the reaction, which in turn reduces surface recombination losses and improves charge utilization.[11] Thus, interpreting photocatalysis through the framework of charge supply and charge transfer inherently accounts for these recombination pathways, establishing a conceptual link between traditional recombination focused analyses and the dynamics of carrier utilization.

The simplicity of our experimental protocol makes it well-suited for high-throughput screening, which can significantly accelerate material discovery and optimization.[30] Implementing this approach in high-throughput formats allows for the rapid assessment of a wide array of materials, facilitating the identification of trends and optimal balances between charge supply and surface catalysis.

5. Conclusions

In this study, we introduced a method to pinpoint whether photocatalytic performance is dominated by charge supply or surface catalysis. By systematically varying both light intensity and reaction temperature, we introduced the concept of the Onset Intensity for Temperature Dependence (OITD), where temperature starts to significantly affects the overall photocatalytic performance. This simple parameter enables a clear distinction between charge-deficient and surface-limited regimes, providing targeted strategies for catalyst optimization.

Comparisons between TiO_2 and ZnO highlight fundamentally different limitations. TiO_2 exhibits a higher OITD, implying

insufficient carrier generation or migration at lower irradiance. In contrast, lower OITD of ZnO indicates that it readily supplies carriers but is hindered by sluggish charge transfer kinetics, suggesting that surface modifications or cocatalyst loading can be effective in addressing the limtitation. Despite similar activities at high irradiance, these diagnostic measurements reveal each material's unique rate-limiting step.

Applying this approach to TiO_2 samples calcined at different temperatures further illustrates its utility in catalyst design. TiO_2 calcined at lower temperatures benefits primarily from enhanced charge supply, highlighting the importance of synthesizing nanoparticles to ensure carriers successfully reach the surface. In contrast, samples calcined at higher temperatures show improved charge transfer kinetics, though the gain in charge supply due to enhanced crystallinity is less pronounced.

Overall, this OITD-based method serves as a powerful tool for decoupling charge supply from surface charge transfer in photocatalysis. By illuminating the root causes of performance barriers, researchers can more effectively tailor strategies such as improving carrier mobility, tuning surface facets, or incorporating cocatalysts to achieve superior photocatalytic activity. Additionally, the straightforward experimental setup lends itself to high-throughput screening, promising to accelerate both fundamental discoveries and practical developments in photocatalysis. Looking ahead, while our approach enables indirect evaluation of carrier accumulation through temperature and intensity dependence, the direct spectroscopic observation of carrier buildup near the OITD threshold would provide further validation of the proposed framework. Development of techniques that enable such detection under realistic, low-intensity photocatalytic conditions remains an important challenge and opportunity for future research.

Data availability

The data supporting this article is included in the ESI.†

Author contributions

Y. C. conceived the study, conducted experiments, and wrote the manuscript. K. Y. contributed to the initial research planning and experimental setup. P. M. and P. P. prepared samples. K. S. performed TEM analysis. E. S. characterized samples. T. W. provided input through discussions. T. T. supervised the research, supported discussions, and facilitated equipment acquisition. All authors proofread and approved the final manuscript.

Conflicts of interest

There are no conflicts to declare.

Acknowledgements

We appreciate the financial support from JSPS Kakenhi (No. 24KJ1201), Leave a Nest grant KYOCERA Corporation award, and JST SPRING (No. JPMJSP2102).

Notes and references

1 T. Takata, J. Jiang, Y. Sakata, M. Nakabayashi, N. Shibata, V. Nandal, K. Seki, T. Hisatomi and K. Domen, *Nature*, 2020, **581**, 411–414.
2 A. Houas, H. Lachheb, M. Ksibi, E. Elaloui, C. Guillard and J.-M. Herrmann, *Appl. Catal., B*, 2001, **31**, 145–157.
3 S. N. Habisreutinger, L. Schmidt-Mende and J. K. Stolarczyk, *Angew. Chem., Int. Ed.*, 2013, **52**, 7372–7408.
4 W.-J. Chun, A. Ishikawa, H. Fujisawa, T. Takata, J. N. Kondo, M. Hara, M. Kawai, Y. Matsumoto and K. Domen, *J. Phys. Chem. B*, 2003, **107**, 1798–1803.
5 J.-C. Wu, J. Zheng, P. Wu and R. Xu, *J. Phys. Chem. C*, 2011, **115**, 5675–5682.
6 X. Chen, L. Liu and F. Huang, *Chem. Soc. Rev.*, 2015, **44**, 1861–1885.
7 Y. Kageshima, S. Shiga, T. Ode, F. Takagi, H. Shiiba, M. T. Htay, Y. Hashimoto, K. Teshima, K. Domen and H. Nishikiori, *J. Am. Chem. Soc.*, 2021, **143**, 5698–5708.
8 R. Wang, Z. Wang, L. Zhang, Q. Wang, Z. Zhao, W. Huang and J. Shi, *ACS Energy Lett.*, 2022, **7**, 1980–1986.
9 J. Yang, D. Wang, H. Han and C. Li, *Acc. Chem. Res.*, 2013, **46**, 1900–1909.
10 J. Zhu, S. Pang, T. Dittrich, Y. Gao, W. Nie, J. Cui, R. Chen, H. An, F. Fan and C. Li, *Nano Lett.*, 2017, **17**, 6735–6741.
11 Y. Cho, T. He, B. Moss, D. Benetti, C. Liang, L. Tian, L. J. F. Hart, A. A. Wilson, Y. Taniguchi, J. Cui, M. Yang, S. Eslava, A. Yamaguchi, M. Miyauchi and J. R. Durrant, *ACS Catal.*, 2024, 16543–16550.
12 Y. Cho, A. Yamaguchi, R. Uehara, S. Yasuhara, T. Hoshina and M. Miyauchi, *J. Chem. Phys.*, 2020, **152**, 231101.
13 A. Mills, *Appl. Catal., B*, 2012, **128**, 144–149.
14 F. Güell, A. Galdámez-Martínez, P. R. Martínez-Alanis, A. C. Catto, L. F. Da Silva, V. R. Mastelaro, G. Santana and A. Dutt, *Mater. Adv.*, 2023, **4**, 3685–3707.
15 F. Amano, K. Nogami, M. Tanaka and B. Ohtani, *Langmuir*, 2010, **26**, 7174–7180.
16 J. T. Carneiro, T. J. Savenije, J. A. Moulijn and G. Mul, *J. Phys. Chem. C*, 2010, **114**, 327–332.
17 S. Naniwa, K. Kato, A. Yamakata, A. Yamamoto and H. Yoshida, *ACS Catal.*, 2023, **13**, 15212–15218.
18 W. Q. Fang, X.-Q. Gong and H. G. Yang, *J. Phys. Chem. Lett.*, 2011, **2**, 725–734.
19 G. Liu, H. G. Yang, J. Pan, Y. Q. Yang, G. Q. Lu and H.-M. Cheng, *Chem. Rev.*, 2014, **114**, 9559–9612.
20 M. Liu, L. Piao, L. Zhao, S. Ju, Z. Yan, T. He, C. Zhou and W. Wang, *Chem. Commun.*, 2010, **46**, 1664–1666.
21 R. Abe, M. Higashi and K. Domen, *J. Am. Chem. Soc.*, 2010, **132**, 11828–11829.
22 C. A. Mesa, M. Sachs, E. Pastor, N. Gauriot, A. J. Merryweather, M. A. Gomez-Gonzalez, K. Ignatyev, S. Giménez, A. Rao, J. R. Durrant and R. Pandya, *Nat. Commun.*, 2024, **15**, 3908.
23 J. Ravensbergen, F. F. Abdi, J. H. van Santen, R. N. Frese, B. Dam, R. van de Krol and J. T. M. Kennis, *J. Phys. Chem. C*, 2014, **118**, 27793–27800.

24 S. D. Dimitrov, M. Azzouzi, J. Wu, J. Yao, Y. Dong, P. S. Tuladhar, B. C. Schroeder, E. R. Bittner, I. McCulloch, J. Nelson and J. R. Durrant, *J. Am. Chem. Soc.*, 2019, **141**, 4634–4643.
25 R. Yanagi, T. Zhao, D. Solanki, Z. Pan and S. Hu, *ACS Energy Lett.*, 2022, **7**, 432–452.
26 Q. Zhang, G. Xie, M. Duan, Y. Liu, Y. Cai, M. Xu, K. Zhao, H. Tai, Y. Jiang and Y. Su, *ACS Appl. Nano Mater.*, 2023, **6**, 17445–17456.
27 J. Ran, M. Jaroniec and S. Qiao, *Adv. Mater.*, 2018, **30**, 1704649.
28 Y. Ham, T. Hisatomi, Y. Goto, Y. Moriya, Y. Sakata, A. Yamakata, J. Kubota and K. Domen, *J. Mater. Chem. A*, 2016, **4**, 3027–3033.
29 Y. Cho, M. Yang, J. Cui, Y. Yang, S. P. Singh, S. Eslava, D. Benetti, J. R. Durrant, A. Yamaguchi, M. Miyauchi and F. Amano, *J. Am. Chem. Soc.*, 2025, **147**(9), 7703–7710.
30 K. Yanagiyama, K. Takimoto, S. Dinh Le, N. Nu Thanh Ton and T. Taniike, *Environ. Pollut.*, 2024, **342**, 122974.